



Mitochondrial temperature-responsive drug delivery reverses drug resistance in lung cancer

Lifo Ruan^{a,b,1}, Jun Chen^{a,b,1}, Chuanchao Du^c, Huiru Lu^a, Jiayu Zhang^a, Xiaomeng Cai^{a,b}, Rui Dou^{a,b}, Wenchu Lin^{d,e}, Zhifang Chai^{a,b}, Guangjun Nie^{b,f,*}, Yi Hu^{a,b,**}

^a CAS Key Laboratory for Biomedical Effects of Nanomaterials and Nanosafety, Multi-disciplinary Research Division, Institute of High Energy Physics, Chinese Academy of Sciences (CAS), Beijing, 100049, PR China

^b University of Chinese Academy of Sciences, Beijing, 100049, PR China

^c Peking University Third Hospital, Beijing, 100191, PR China

^d High Magnetic Field Laboratory, Hefei Institutes of Physical Science, Chinese Academy of Sciences, Hefei, 230031, Anhui, PR China

^e University of Science and Technology of China, Hefei, 230026, Anhui, PR China

^f CAS Key Laboratory for Biomedical Effects of Nanomaterials and Nanosafety, CAS Center for Excellence in Nanoscience, National Center for Nanoscience and Technology, Beijing, 100190, PR China

ARTICLE INFO

Keywords:

Mitochondrial temperature
Thermoresponsive
Drug delivery
Drug resistance
Nanomedicines

ABSTRACT

Reversal of cancer drug resistance remains a critical challenge in chemotherapy. Mitochondria-targeted drug delivery has been suggested to mitigate drug resistance in cancer. To overcome the intrinsic limitations in conventional mitochondrial targeting strategies, we develop mitochondrial temperature-responsive drug delivery to reverse doxorubicin (DOX) resistance in lung cancer. Results demonstrate that the thermoresponsive nanocarrier can prevent DOX efflux and facilitate DOX accumulation and mitochondrial targeting in DOX-resistant tumors. As a consequence, thermoresponsive nanocarrier enhances the cytotoxicity of DOX and reverses the drug resistance in tumor-bearing mice. This work represents the first example of mitochondrial temperature-responsive drug delivery for reversing cancer drug resistance.

1. Introduction

Drug resistance is still one of the principal obstacles for the chemotherapy against cancer [1,2]. For instance, small-cell lung cancer nearly always relapses with drug resistance after the initial chemotherapy [3]. Although the mechanisms underlying cancer drug resistance remain incompletely understood, multiple lines of evidence suggest that ATP-binding cassette transporters might be implicated in drug resistance in a tumor type-dependent fashion [4]. Since these transporters are mainly ATP-driven multidrug efflux pumps (multidrug resistance protein (MRP), P-glycoprotein (P-gp)) [5], sabotage of ATP production would be a promising strategy for reversing drug resistance.

Mitochondria are the intracellular power plant that houses ATP-synthesizing machinery [6,7]. A critical role of mitochondria emerges in multidrug-resistant cancers [8], and targeted drug delivery to

mitochondria has recently attracted much attention [9–20]. Delocalized lipophilic cations (DLCs) have been commonly harnessed for mitochondrial targeting [21]. Although mitochondrial membranes in cancer cells are generally more negatively charged than those in healthy cells, the difference could be rather small [22]. As such, DLCs-based targeting strategy could not specifically target the mitochondria in cancer cells. Moreover, *in vivo* imaging has suggested that considerable heterogeneity of mitochondrial membrane potential exists within individual lung tumors [23], which inevitably compromises the targeting efficacy of DLCs to mitochondria in tumors. Therefore, mitochondrial targeting that does not rely on mitochondrial membrane potential may bypass those limitations.

It has been recently reported that active mitochondria can be physiologically maintained at approximately 48 °C [24]. Moreover, the difference in mitochondrial temperatures has been suggested to exist

Peer review under responsibility of KeAi Communications Co., Ltd.

* Corresponding author. National Center for Nanoscience and Technology, Beijing, 100190, PR China.

** Corresponding author. Institute of High Energy Physics, Beijing, 100049, PR China.

E-mail addresses: niegj@nanocr.cn (G. Nie), huyi@ihep.ac.cn (Y. Hu).

¹ These authors contributed equally to this work.

<https://doi.org/10.1016/j.bioactmat.2021.10.045>

Received 11 August 2021; Received in revised form 12 October 2021; Accepted 29 October 2021

Available online 4 November 2021

2452-199X/© 2021 The Authors. Publishing services by Elsevier B.V. on behalf of KeAi Communications Co. Ltd. This is an open access article under the CC

BY-NC-ND license (<http://creativecommons.org/licenses/by-nc-nd/4.0/>).

between normal cells and cancer cells [25]. Such difference might help circumvent the potential obstacles in nanodrug circulation [26] and thus facilitate the specific targeting to mitochondria in cancer cells. Herein, we took advantage of mitochondrial temperature-responsive nanocarrier to reverse drug resistance in small-cell lung cancer (Scheme 1). As the demands for reversing drug-resistant cancer continue to rise, it represents a must-do application of thermoresponsive drug delivery to combat cancer drug resistance.

2. Experimental section

2.1. Preparation and characterization of nanocarriers

We first synthesized the macromolecular crosslinker as follows. Briefly, 1,6-Hexanediol diacrylate (452.5 mg, 2 mmol) and 4-(Amino-methyl)piperidine (114.2 mg, 1 mmol) were added in a bottle containing 5 mL of DMSO and stirred for three days at 60 °C under argon protection. Poly(β -aminoester)s containing acrylates as end groups were obtained and stored in dark at –20 °C prior to use. Poly(*N*-isopropylacrylamide) (PNIPAM)- and polyacrylamide (PAM)-derived nanocarriers were prepared as follows. *N*-isopropylacrylamide (226 mg, 2 mmol) or acrylamide (142 mg, 2 mmol), crosslinker (250 μ L, 0.05 mmol), poly(ethylene glycol) methyl ether methacrylate (240 mg, 0.25 mmol), sodium dodecyl sulfate (20 mg, 0.07 mmol), *N*-(3-Aminopropyl) methacrylamide hydrochloride (14.3 mg, 0.08 mmol) and *N,N*-Methylenebis(acrylamide) (3 mg, 0.02 mmol) were added in 20 mL of ddH₂O and stirred with argon protection. The initiator ammonium persulfate (22.8 mg, 0.1 mmol) was used to react for 4 h at 70 °C under argon protection, followed by purification of the nanoparticles through dialysis (MWCO = 10000 Da). Afterward, the nanoparticles were conjugated with (4-Carboxybutyl)triphenylphosphonium bromide (TPP) (a mass ratio of 25:1) through EDC/NHS-assisted coupling reaction. After being dialyzed with ddH₂O for 24 h, the nanoparticles were mixed with 6-Maleimidohexanoic acid *N*-hydroxysuccinimide ester at a mass ratio of 35:1 at 30 °C for 30 min. Afterward, iRGD was mixed with the nanoparticles at a mass ratio of 1:10 overnight at 30 °C. The nanoparticles were dialyzed in ddH₂O for 24 h (MWCO = 3500 Da) to remove free iRGD and collected by lyophilization. PNIPAM/iRGD and PAM/iRGD nanocarriers were prepared as described above without TPP decoration step. PNIPAM (no crosslinker) nanocarrier was prepared as described above except that the crosslinker was replaced by poly(ethylene glycol) methyl ether methacrylate (48 mg, 0.05 mmol).

The asprepared nanocarriers were characterized by NMR and FTIR. The morphology of nanocarriers was analyzed by TEM. The nanocarriers were dispersed in deionized water (200 μ g/mL) and sonicated for 15 min before DLS measurements at 25 °C. TEM samples were prepared by the

phosphotungstic acid staining method as previously reported [14]. The lower critical solution temperature (LCST) of the nanoparticles was determined with pyrene fluorescence according to an established procedure [14].

For cell imaging experiments, the fluorescently labeled nanocarriers were prepared as follows: 10 mg of the nanoparticles and Cy5 NHS (200 μ g, 0.3 μ mol) were incubated in 2 mL DMSO for 24 h, followed by the dialysis in ddH₂O for 24 h (MWCO = 3500 Da).

2.2. Doxorubicin (DOX) loading

The DOX loading into PNIPAM nanoparticles (DOX@PNIPAM) and PAM nanoparticles (DOX@PAM) was carried out by using a solvent replacement method as previously described [27]. Briefly, DOX•HCl (20 mg) was firstly stirred with 1.5 equivalence of triethylamine in 1 mL of DMSO for 2 h to remove HCl, followed by addition of 10 mL of ethanol solution containing 20 mg of the nanocarriers with sonication. The nanoparticles were purified by dialysis in ddH₂O for 24 h.

Formula of drug loading efficiency (DLE) and drug loading content (DLC):

$$DLE(\%) = \frac{\text{weight of feeding DOX} - \text{weight of DOX in dialysate}}{\text{weight of feeding DOX}} \times 100\%$$

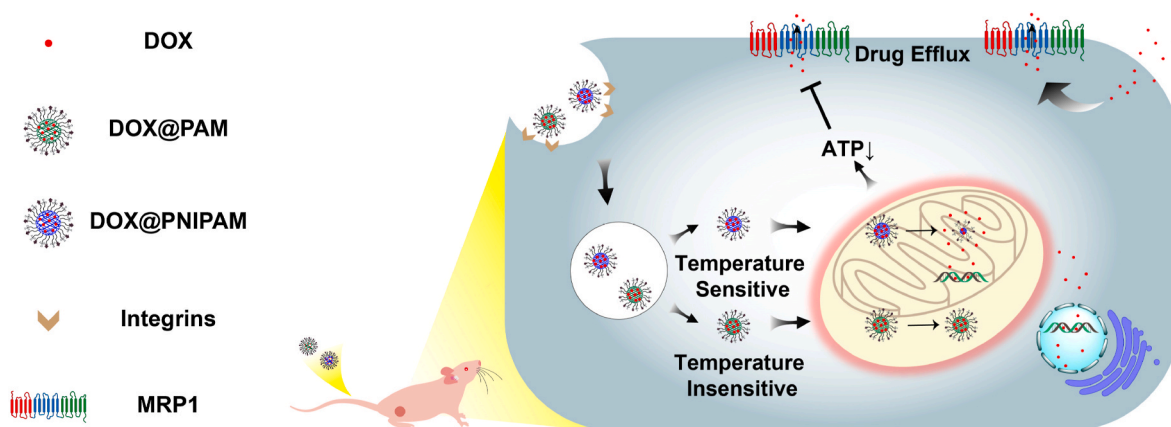
$$DLC(\%) = \frac{\text{weight of feeding DOX} - \text{weight of DOX in dialysate}}{\text{weight of nanoparticles}} \times 100\%$$

2.3. DOX release in solutions

DOX release from the nanoparticles in PBS was examined as follows. The nanoparticles were incubated in PBS at 25 °C, 37 °C, 40 °C, 42 °C, 44 °C or 48 °C for different time. After the incubation, the solutions were centrifuged (10 000 rpm) for 1 min, and the supernatant was obtained for DOX measurement at 480 nm. After the DOX analysis each time, PBS solution was refilled to disperse the nanoparticles for further incubation.

2.4. Inhibition of tumor cells

H69AR or H69 cells were cultured in 96-well plates overnight. Different concentrations of the nanoparticles were added and incubated with the cells. After 24 h, the cell culture medium was removed. MTT solution was added and incubated with the cells at 37 °C for another 4 h. Afterward, the medium was removed and 100 μ L of DMSO was added. A microplate reader was used to record the solution absorbance at 570 nm.



Scheme 1. Scheme of mitochondrial temperature-responsive drug delivery in a DOX-resistant model of small-cell lung cancer. In contrast to nonthermoresponsive nanocarrier PAM, thermoresponsive nanocarrier PNIPAM can release DOX upon high mitochondrial temperature, which consequently damages mitochondria and reverses DOX resistance.

Cell viability was analyzed according to the solution absorbance.

2.5. Intracellular DOX levels

After H69AR cells were cultured for 24 h, the fresh medium containing DOX-loaded nanoparticles was added to the cells and incubated for 12–48 h. After PBS washing, a fresh medium was added, followed by the staining of cell nuclei. Confocal laser scanning microscopy was used to image intracellular DOX fluorescence that was further analyzed by ImageJ.

2.6. Lysosomal escape

After H69AR cells were cultured for 24 h, Cy5-labeled nanocarriers were incubated with H69AR cells for 1 h or 4 h. After PBS washing, a fresh medium was added to H69AR cells. LysoTracker Green and Hoechst 33342 were used to stain the lysosomes and cell nuclei, respectively, according to the manufacturers' protocols. Confocal laser scanning microscopy was used to image the lysosomes and the nanocarriers. Pearson's correlation coefficient for colocalization was obtained from NIS-Elements Viewer.

2.7. Mitochondria targeting of nanocarriers

After H69AR cells were cultured for 24 h, Cy5-labeled nanocarriers were incubated with cells for another 12 h. After PBS washing, a fresh medium was added to H69AR cells. Mitotracker Green was used to stain the mitochondria for 30 min. Confocal laser scanning microscopy was used to image the mitochondria and the nanocarriers. Pearson's correlation coefficient for colocalization was obtained from NIS-Elements Viewer.

2.8. Mitochondrial targeting of DOX-loaded nanoparticles

After H69AR cells were cultured for 24 h, DOX-loaded nanoparticles or the control samples were incubated with H69AR cells for 12 h. After PBS washing, mitochondrial staining with Mitotracker Green was conducted as described above. Confocal laser scanning microscopy was used to image DOX and the mitochondria. Pearson's correlation coefficient for colocalization was obtained from NIS-Elements Viewer.

2.9. Mitochondrial membrane potential

After 24 h cell culture, DOX-loaded nanoparticles were incubated with H69AR cells for 24 h. Afterward, JC-1 staining was conducted following the manufacturer's protocols. Intracellular fluorescence was quantified by ImageJ. The red/green fluorescence ratios were calculated by OriginPro 2017. The conversion of red fluorescence (aggregates) to green fluorescence (monomers) indicates mitochondrial depolarization.

2.10. Intracellular ATP level

An ATP assay kit was used to analyze the intracellular ATP levels [28]. H69AR cells were cultured for 24 h and then incubated with DOX-loaded nanoparticles (equivalent of 20 µg/mL DOX) for another 24 h. After the incubation, 200 µL of cell lysis buffer was used to lyse H69AR cells, followed by the centrifugation (12 000 rpm, 4 °C) for 5 min. The ATP levels in the supernatants were analyzed with the ATP assay kit.

2.11. In vivo biodistribution of Cy5-labeled nanocarriers and DOX

100 µL of free Cy5 or Cy5-labeled nanocarriers (Cy5 concentration, 20 µg/mL) were intravenously injected into the BALB/c nude mice bearing H69AR tumors. Fluorescent images were recorded at 1, 6, and 24 h post injections with *in vivo* imaging system (Ex/Em = 640/680 nm).

For DOX imaging in organs, 100 µL of free DOX and the nanoparticles (DOX concentration, 1.6 mg/mL) were administrated in mice. After 24 h, the imaging of tumors and major healthy organs from the mice was carried out to analyze the DOX fluorescence (Ex/Em = 465/580 nm).

2.12. In vivo evaluation of the antitumor effects of DOX@PNIPAM

In vivo evaluation of the antitumor effects of nanodrugs was conducted in BALB/c nude mice bearing H69AR tumors. Briefly, 1.0×10^7 cells/100 µL of H69AR cells were inoculated in the right flank of BALB/c nude mice (4–6 weeks, female, 16 ± 2 g, Beijing WeiTongLiHua Animal Co. Ltd., Beijing, China). When the tumors were ~ 50 mm³, the mice were randomly grouped for the following experiments. Free DOX, DOX@PAM or DOX@PNIPAM (equivalent dose of 8 mg/kg of DOX) was intravenously injected into the mice every three days. After the injections, the tumor growth in mice was recorded every three days. Relative mouse weight was determined as M/M_0 , where M_0 was the initial weight. After the treatments, tumors and the major healthy organs were collected from the mice. Hematoxylin and eosin (H&E) and Ki-67 assays were performed to examine the antitumor effects as previously described [27].

3. Results and discussion

3.1. Preparation and characterization of nanocarriers

Poly(*N*-isopropylacrylamide) (PNIPAM) was used to construct a thermoresponsive nanocarrier, while polyacrylamide (PAM) was a nonthermoresponsive control. The nanocarriers were prepared via a step-by-step synthetic routine. First, an acrylate-terminal hyperbranched poly(β -amino ester) (PAE) was synthesized to serve as the macromolecular crosslinker. Fourier-transform infrared (FTIR) analysis validated the existence of PAE crosslinker in obtained nanocarriers through the appearance of the characteristic absorbance bands of 1735 cm⁻¹ ascribed to carbonyl bonds stretching in ester groups and the intensity increment of absorbance bands between 1360 and 1300 cm⁻¹ ascribed to C–N bonds vibration for tertiary amines (Fig. S1). The PAE crosslinker not only provides the hydrophobic domain for the nanocarriers to encapsulate DOX, but also facilitates mitochondrial targeting of the nanoparticles. Next, the amino groups were introduced into the nanocarriers for further modifications using *N*-(3-Aminopropyl)methacrylamide. TPP was conjugated to the nanocarriers by EDC/NHS reactions. FTIR results showed the decoration of TPP on the nanoparticle surface through the appearance of multiple absorbance bands at 1400–1600 cm⁻¹ corresponding to the typical skeletal vibrations of benzene (Fig. S2). The appearance of the typical peak at ~ 7.2 ppm in ¹H NMR spectra indicated the existence of the phenyl groups in the nanoparticles (Fig. S3). Furthermore, the nanocarriers were conjugated with iRGD by utilizing *N*-Succinimidyl 6-maleimidohexanoate as a linker. iRGD is a disulfide-bridged cyclic peptide that can facilitate the nanoparticles to target and penetrate solid tumors [29]. The appearance of a broad band from 3600 to 3400 cm⁻¹ was resulted from the typical stretching vibration of N–H bonds in primary amines of iRGD (Fig. S2), suggesting the successful decoration of iRGD to the nanocarriers. Therefore, FTIR and ¹H NMR validated the decoration of iRGD and TPP onto the nanocarriers.

The uniform spherical morphology of PNIPAM-derived (Fig. 1a) and PAM-derived nanocarriers (Fig. 1b) was illustrated by transmission electron microscopy (TEM). Dynamic light scattering (DLS) analysis indicated that the average size of the PNIPAM-derived nanocarriers increased to ~ 286 nm after DOX loading (Fig. S4a), and DOX-loaded PAM was ~ 299 nm (Fig. S4b). After DOX was encapsulated into the nanocarriers, the characteristic DOX peak at ~ 480 nm was still found in the UV–vis spectra (Fig. S5), suggesting the DOX loading into the nanocarriers. The drug loading efficiency (DLE) of DOX@PNIPAM nanoparticles was $\sim 72.7\%$, while drug loading content (DLC) was

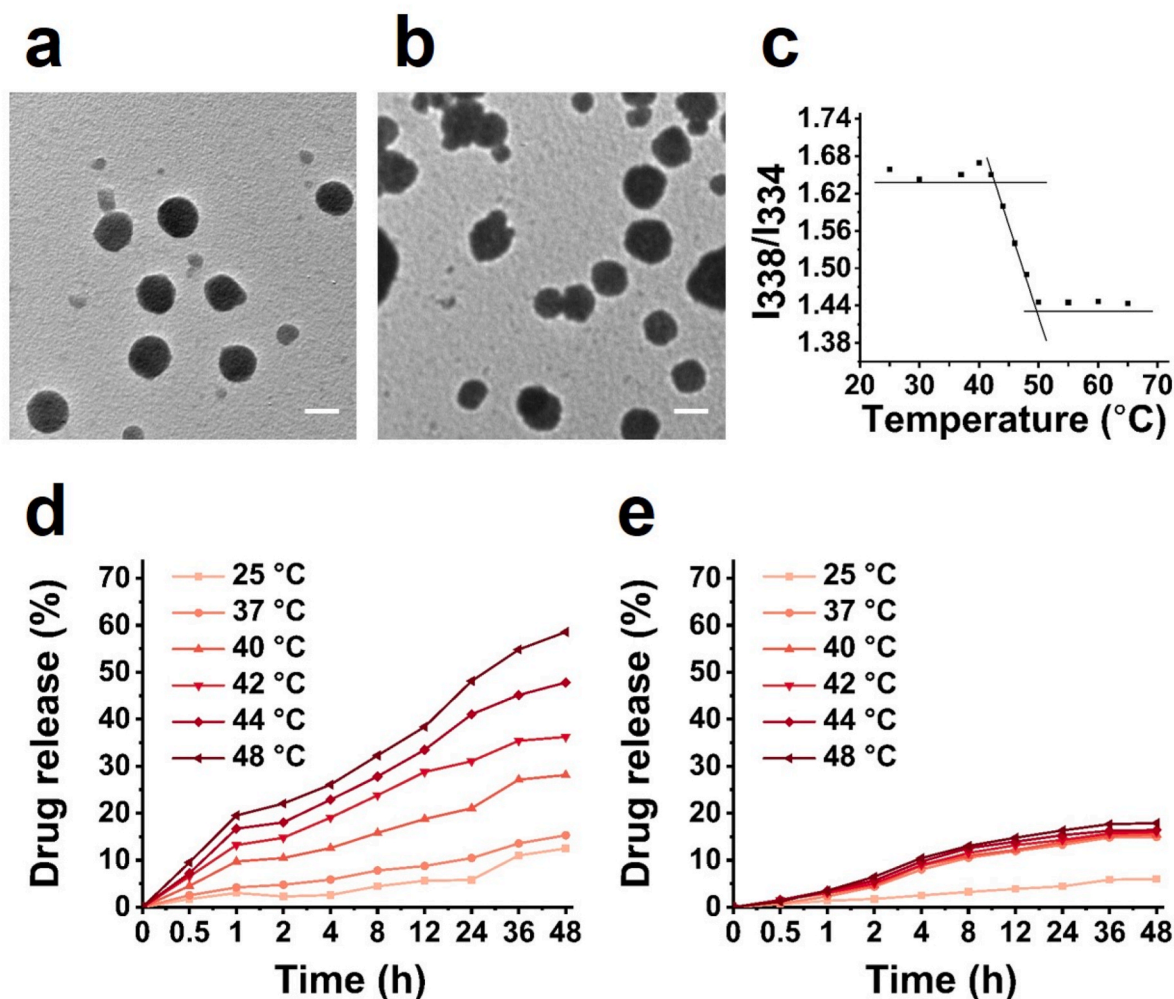


Fig. 1. TEM images of PNIPAM-derived nanocarriers (a) and PAM-derived nanocarriers (b). Scale bar = 200 nm. (c) Characterization of LCST of PNIPAM-derived nanocarriers (2 mg/mL) by pyrene fluorescence spectroscopy. DOX release from DOX@PNIPAM (d) and DOX@PAM (e) at 25 °C, 37 °C, 40 °C, 42 °C, 44 °C and 48 °C.

~36.4%. DLE and DLC of DOX@PAM were around 75.3% and 37.7%, respectively.

To be suitable for mitochondrial temperature-responsive drug delivery, LCST of PNIPAM-derived nanocarrier was well adjusted to ~48 °C by adding an appropriate amount of polyethylene glycol (PEG) derivative (Fig. 1c). Furthermore, the temperature-responsive property of the nanoparticle was characterized after loading DOX. DOX release from DOX@PNIPAM and DOX@PAM was examined at different temperatures. As shown in Fig. 1d, ~12.5% of DOX was released from DOX@PNIPAM after 48 h at 25 °C. When the temperature increased, DOX release increased in a temperature-dependent fashion. At 48 °C, cumulative DOX release from DOX@PNIPAM increased to approximately 58.6% after 48 h. In contrast to DOX release from DOX@PNIPAM, DOX release from the nonthermosensitive control DOX@PAM was up to ~17.9% at 48 °C (Fig. 1e). These results confirmed the thermoresponsive release of DOX from DOX@PNIPAM *in vitro*.

3.2. Mitochondria-targeted DOX delivery by DOX@PNIPAM

Mitochondria-targeted DOX delivery was analyzed by staining mitochondria with MitoTracker. Results showed that the colocalization of free DOX with mitochondria was poor (Fig. 2a). In contrast to free DOX, both DOX@PNIPAM and DOX@PAM could enhance the colocalization of DOX with mitochondria (Fig. 2a). Further analysis indicated that DOX was colocalized with mitochondria to a lesser extent in DOX@PAM group (Pearson's correlation coefficient, 0.75) than in

DOX@PNIPAM group (Pearson's correlation coefficient, 0.94) (Fig. 2b). In addition, we examined the mitochondrial targeting of TPP-DOX (Fig. S6) in H69AR cells. Results showed that TPP-DOX was poorly colocalized with mitochondria (Pearson's correlation coefficient, 0.67) (Fig. 2b), suggesting that TPP alone is not sufficient to deliver DOX to mitochondria in H69AR cells. These results highlighted the advantage of PNIPAM-based nanocarrier for enhancing the colocalization of DOX with mitochondria.

We next asked whether the difference in DOX colocalization with mitochondria between DOX@PNIPAM and DOX@PAM groups was derived from the mitochondrial targeting capacities of the two nanocarriers. The nanocarriers were labeled with Cy5 for cell imaging. The mitochondrial colocalization of PAM-Cy5 (Pearson's correlation coefficient, 0.81) was comparable to that of PNIPAM-Cy5 (Pearson's correlation coefficient, 0.80) (Fig. 2c). In the nanocarriers, TPP can help the nanoparticles escape from lysosomes [30]. The lysosomal escape capacities of the nanocarriers were confirmed by examining the colocalization of the nanoparticles with lysosomes over time (Fig. S7). Moreover, TPP could assist in the colocalization of the nanocarriers with mitochondria, as suggested by the negative controls (Fig. S8). Similarly, the PAE crosslinker as cationic polymers also facilitated the mitochondrial targeting of the nanocarriers (Fig. S9). These results suggested that both nanocarriers could moderately target the mitochondria to a similar extent. Apart from the mitochondrial targeting capacities of the nanocarriers, the thermoresponsive DOX@PNIPAM could further facilitate DOX delivery to mitochondria. To further verify the high temperature of

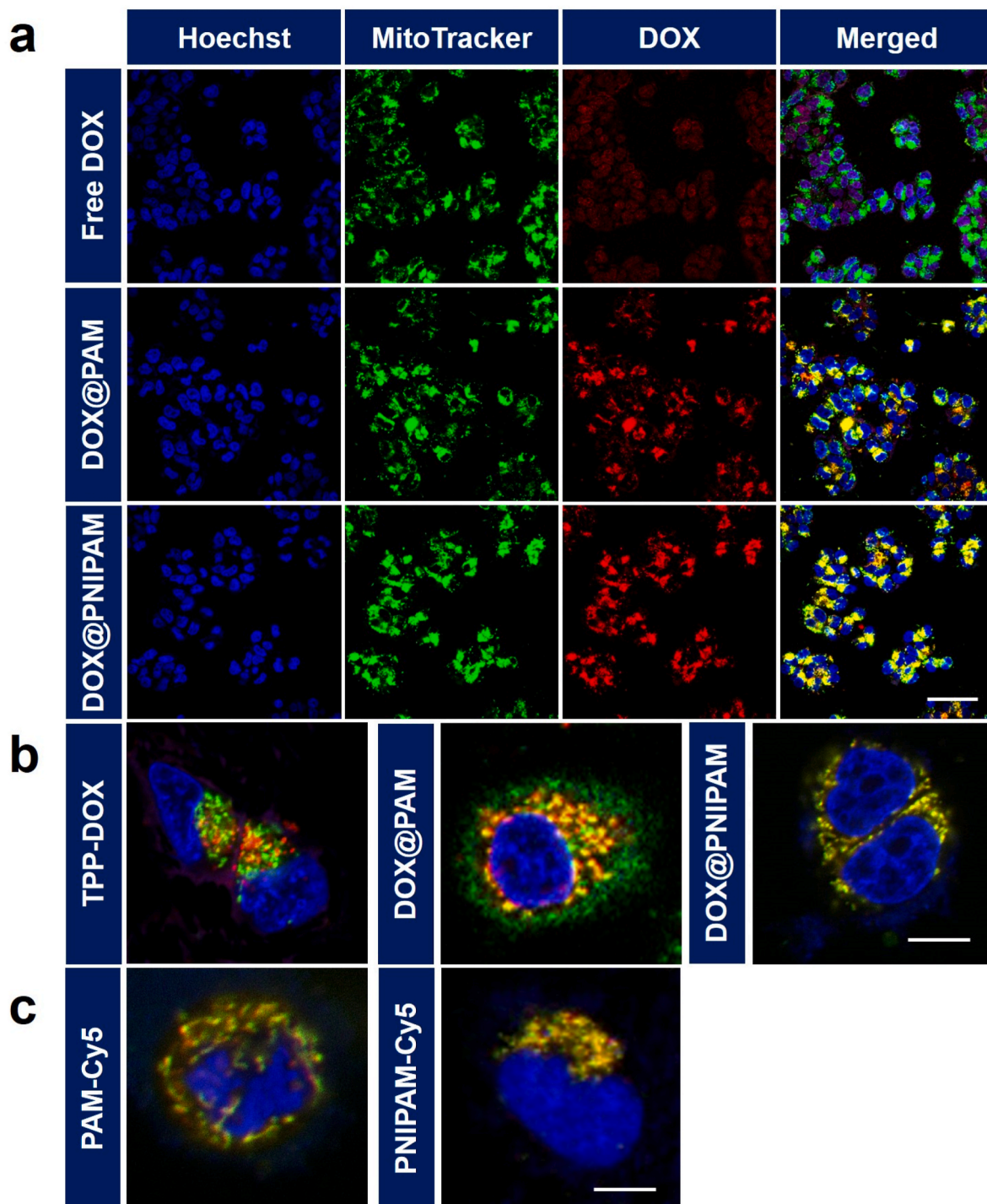


Fig. 2. (a) Confocal images of H69AR cells incubated with 10 µg/mL of DOX or DOX-loaded nanoparticles (containing 10 µg/mL of DOX) for 12 h. Scale bar = 50 µm. (b) Colocalization analysis of mitochondria (green) with TPP-DOX, DOX@PAM and DOX@PNIPAM (equivalent dose of 10 µg/mL of DOX) after 12 h incubation. Scale bar = 10 µm. (c) Colocalization analysis of mitochondria (green) and Cy5-labeled nanocarriers (Cy5 concentration, 1 µg/mL, red) after 12 h incubation of the nanocarriers with the cells. Scale bar = 10 µm. The cell nuclei were visualized by Hoechst 33342 (blue).

mitochondria in H69AR cells, we used a temperature-sensitive and mitochondria-targeted fluorescent probe to compare the mitochondrial temperature between H69AR cells and a normal cell line (human umbilical vein endothelial cells, HUVEC) [31]. Results indicated that the mitochondrial temperature in H69AR cells could be relatively higher than that in HUVEC (Fig. S10).

Subsequently, the intracellular DOX levels in H69AR cells were examined. As shown in Fig. S11, DOX fluorescence was much weaker in free DOX group than in the other two groups, suggesting that free DOX

could not be retained in H69AR cells. By contrast, time-dependent accumulation of DOX inside H69AR cells was found in DOX@PNIPAM group, suggesting that DOX@PNIPAM might inhibit the efflux of DOX from H69AR cells (Fig. S12).

3.3. *In vitro* antitumor effects of DOX@PNIPAM

DOX accumulation in DOX-resistant cells was a positive sign of reversing DOX resistance. We then examined the cytotoxicity of

DOX@PNIPAM in H69AR cells. H69AR is a cellular model of DOX-resistant small-cell lung cancer. Compared with the parental H69 cells, H69AR is approximately 32-fold resistant to DOX [32], and therefore H69AR represents one of the highly DOX-resistant cell lines [33]. In H69AR cells, the overexpression of MRP1, instead of P-gp, is considered most responsible for DOX resistance [34,35]. H69AR cells were incubated with different samples for 24 h, followed by the cytotoxicity assays. Results showed that DOX@PNIPAM was considerably more cytotoxic to H69AR cells than free DOX or DOX@PAM (Fig. 3a). Similarly, the potent antitumor effect of DOX@PNIPAM was also found in H69 cells (Fig. S13). IC_{50} of DOX@PNIPAM was approximately 35 $\mu\text{g}/\text{mL}$ for H69AR cells, which was much lower than IC_{50} of DOX@PAM (>100 $\mu\text{g}/\text{mL}$). The relatively high cytotoxicity of DOX@PNIPAM was in agreement with increased intracellular DOX accumulation and enhanced DOX colocalization with mitochondria by DOX@PNIPAM. Besides the enhanced DOX colocalization with mitochondria, DOX levels in nuclei were also increased by DOX@PNIPAM (Fig. S11). Because the main targets of DOX are DNA and topoisomerase II that reside in both nuclei and mitochondria [36,37], thermoresponsive release of DOX and subsequent DOX accumulation in nuclei/mitochondria may account for the enhanced cytotoxicity of DOX@PNIPAM. Collectively, these results indicated that the thermoresponsive nanocarrier could enhance DOX accumulation in mitochondria and consequently reverse drug resistance. In addition, the nanocarriers were not cytotoxic (Fig. 3b), and they were generally biocompatible as suggested by hemolysis assays (Fig. 3c and d).

3.4. Mechanisms of overcoming drug resistance

In light of the cytotoxicity of DOX@PNIPAM, we next asked whether mitochondria-targeted delivery of DOX would alter mitochondrial membrane potential. JC-1 assays were carried out after H69AR cells were incubated with DOX or the nanoparticles for 24 h. Both DOX@PAM and DOX@PNIPAM could considerably depolarize mitochondrial membranes (Fig. 4a). This is because accumulation of DOX in mitochondria can induce mitochondrial oxidative damage [38]. Mitochondria were more depolarized in DOX@PNIPAM group than in DOX@PAM group (Fig. 4b), which was consistent with higher accumulation of intracellular DOX in DOX@PNIPAM group. Moreover, mitochondrial depolarization disfavoured the electrostatic interactions between the positively charged nanoparticles and mitochondrial membranes, and therefore adversely affected mitochondrial targeting of the nanoparticles. Despite mitochondrial depolarization, DOX@PNIPAM, as compared with DOX@PAM, could still enhance DOX accumulation in mitochondria (Fig. 2), suggesting that thermoresponsive delivery DOX to mitochondria was less compromised by mitochondrial depolarization.

Subsequently, we examined ATP levels in H69AR cells upon the treatments. Results showed that intracellular ATP levels were significantly reduced by DOX@PNIPAM (Fig. 5a). Since ATP-driven transporters pump out intracellular drugs typically against the concentration gradient at the expense of ATP hydrolysis, reduced ATP levels can adversely affect the activity of ATP-dependent drug efflux pumps [8,28]. Rhodamine 123 (Rh123) assays indicated that the activity of drug efflux pumps in H69AR cells was attenuated by DOX@PNIPAM (Figs. 5b and

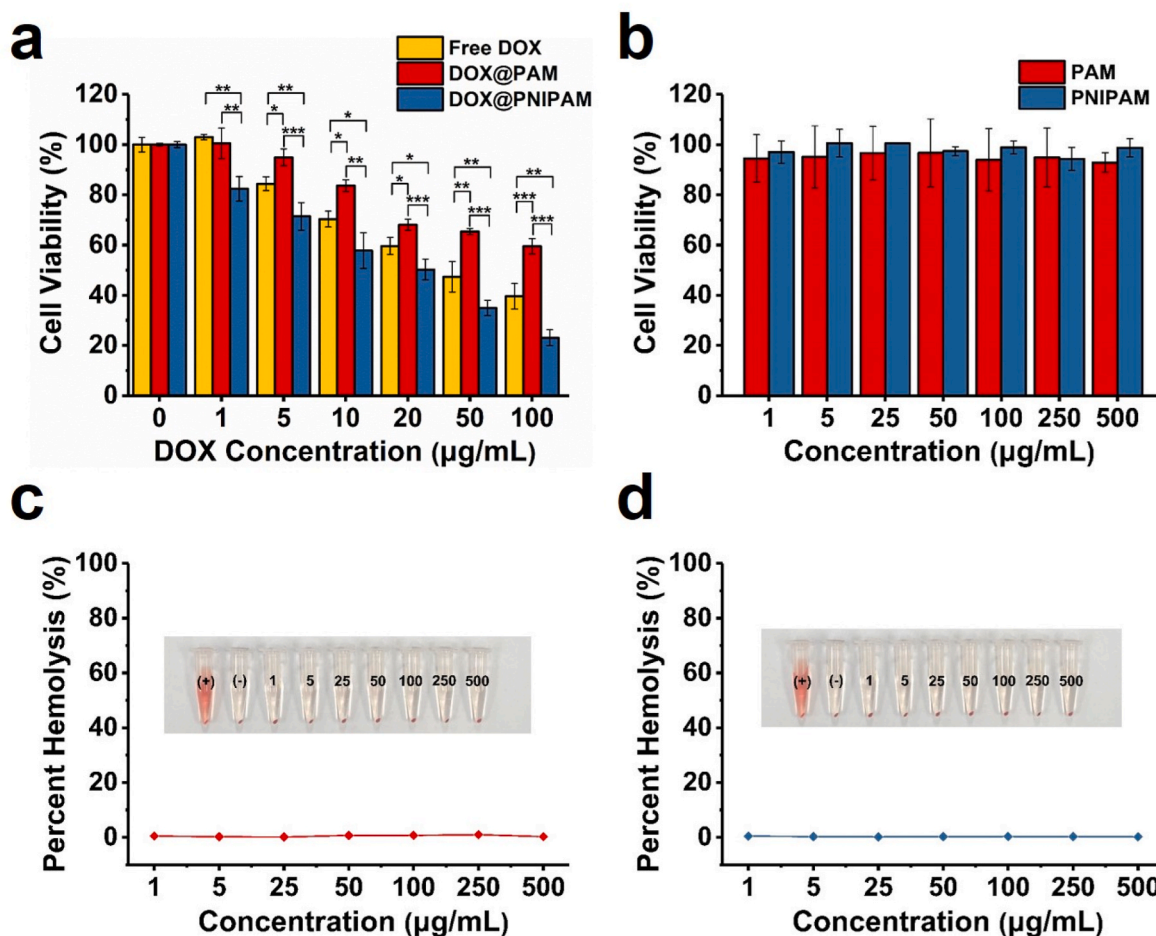


Fig. 3. (a) Cytotoxicity of free DOX and the nanoparticles was determined in H69AR cells at 24 h of incubation. *, $P < 0.05$; **, $P < 0.01$; ***, $P < 0.001$. (b) Cell viability was examined in H69AR cells treated with the nanocarriers at 24 h. Percent hemolysis of red cell suspension incubated with PAM-derived nanocarriers (c) and PNIPAM-derived nanocarriers (d) at 37 °C for 1 h. Deionized water was used as a positive control of hemolysis, while PBS was a negative control.

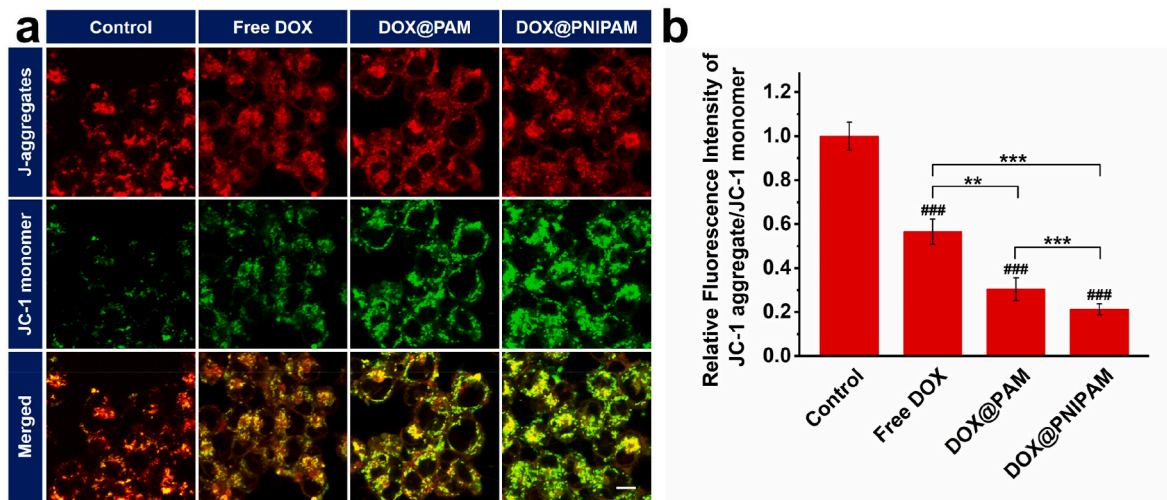


Fig. 4. (a) Confocal microscopic images of JC-1 staining in H69AR cancer cells after 24 h incubation with DOX or DOX-loaded nanoparticles (containing 20 $\mu\text{g}/\text{mL}$ of DOX). Scale bar = 10 μm . (b) Red/green fluorescence ratio of JC-1 in (a). ###, $P < 0.001$ as compared with the control; **, $P < 0.01$; ***, $P < 0.001$ between two treatment groups.

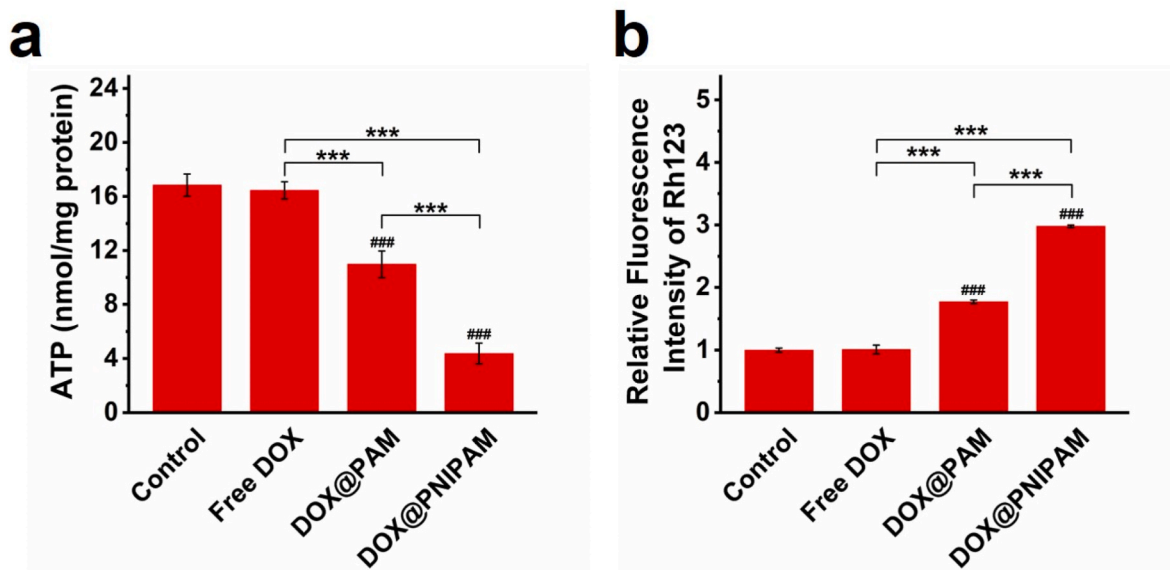


Fig. 5. The effects of DOX or DOX-loaded nanoparticles (containing 20 $\mu\text{g}/\text{mL}$ of DOX) on intracellular ATP (a) and inhibition of Rh123 efflux (b) were shown. ###, $P < 0.001$ as compared with the control; ***, $P < 0.001$ between two treatment groups.

S14), which was in agreement with DOX accumulation in DOX@PNIPAM-treated cells (Fig. S11). Similarly, DOX@PNIPAM treatment increased the intracellular glutathione (GSH) levels in H69AR cells, as compared with the DOX group (Fig. S15). These results suggested that thermoresponsive delivery of DOX to mitochondria can reduce ATP production and consequently inhibit drug efflux in H69AR cells.

3.5. *In vivo* antitumor effects of DOX@PNIPAM

A DOX-resistant mouse model was established by inoculation of H69AR cells in mice. Cy5-labeled nanocarriers were used to analyze the *in vivo* distribution of the nanocarriers at 1, 6 and 24 h. Results showed that *in vivo* fluorescence of Cy5 increased in tumor regions of nanocarriers-treated mice over time, whereas the fluorescence in free Cy5 group fluorescence was barely seen (Fig. S16). Tumor targeting capacity could be ascribed to the iRGD moiety of the nanocarriers

(Fig. S17). Furthermore, we examined DOX distribution in mice treated with free DOX or the nanoparticles. *Ex vivo* images of different mouse organs indicated that DOX@PNIPAM could enhance DOX accumulation in tumors while decreasing DOX levels in heart (Fig. S18). Since cardiotoxicity is the primary adverse effect of DOX [38], reducing DOX in heart tissues can help reduce the adverse effects of the nanodrugs.

The antitumor effects of DOX-loaded nanoparticles were examined after intravenous injections in tumor-bearing mice. Tumor growth profiles of the mice indicated that only DOX@PNIPAM could potently suppress tumor growth in mice (Fig. 6a). Both free DOX and DOX@PAM could hardly suppress the tumor growth. The body weights of mice implied that there was no excessive systemic toxicity in all the treatment groups (Fig. 6b), which was in line with the low cytotoxicity of the nanocarriers (Fig. 3). In addition, blood routine analysis also suggested minimal systemic toxicity (Fig. S19). H&E staining indicated minimal lesions to healthy organs after the treatments (Fig. S20). These results suggested that the nanodrugs were generally biocompatible. After the

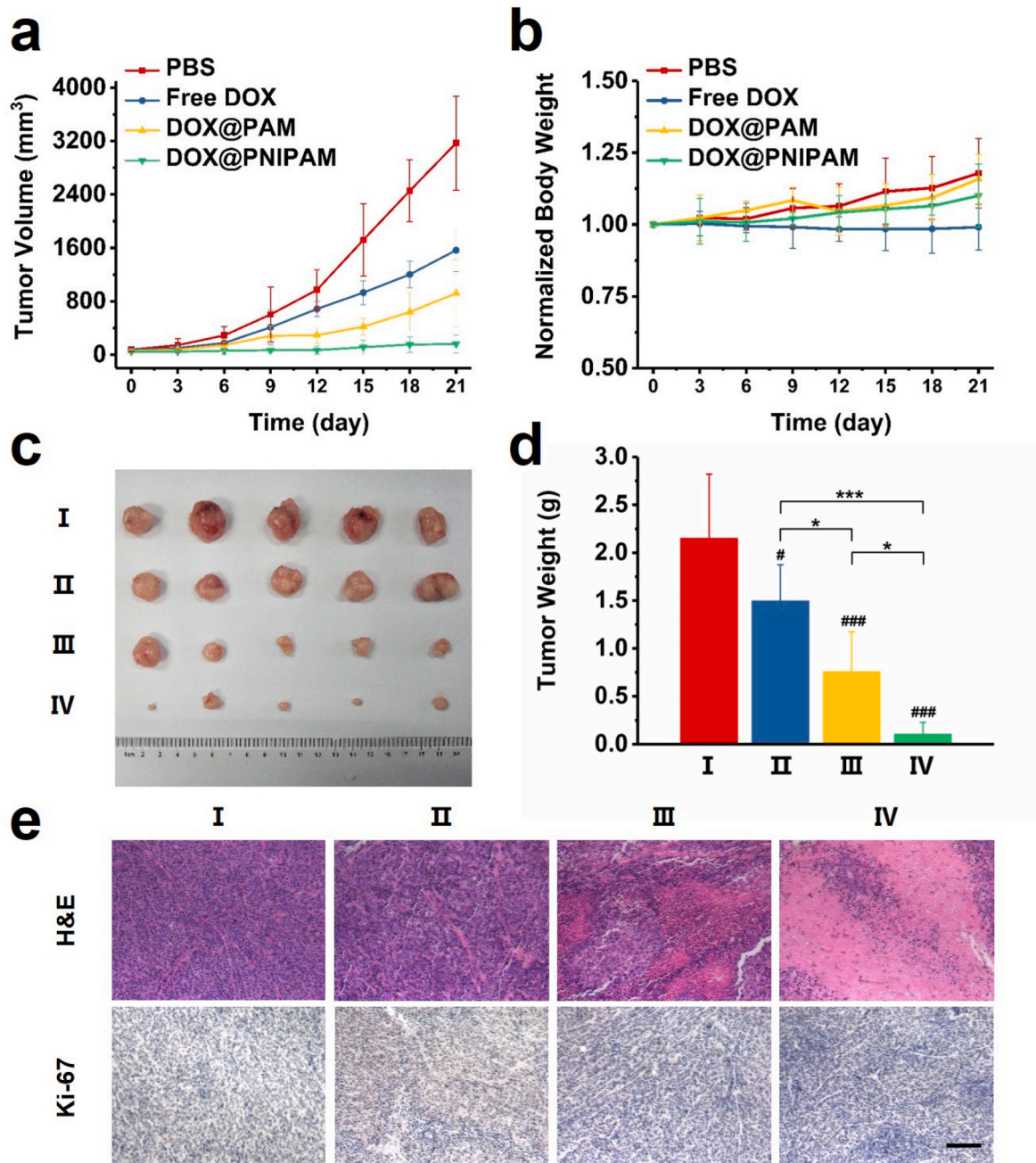


Fig. 6. (a) Tumor growth profiles of the mice following the treatments with PBS, free DOX, DOX@PAM and DOX@PNIPAM (equivalent dose of DOX of 8 mg/kg of body weight). (b) The body weights of mice were monitored every three days. (c) Photos of the tumors excised from the mice after the treatments. (I) PBS, (II) free DOX, (III) DOX@PAM, (IV) DOX@PNIPAM. (d) The tumor weight of each group was averaged (mean \pm SD, $n = 5$). #, $P < 0.05$; ###, $P < 0.001$ between indicated group and the control; *, $P < 0.05$; ***, $P < 0.001$ between indicated groups. (e) H&E and Ki-67 stainings of the tumors. Scale bar = 50 μ m.

treatments, the shrinkage of the tumors from the mice further corroborated the antitumor effects of DOX@PNIPAM (Fig. 6c and d). Stainings of tumor sections with H&E or Ki-67 also indicated DOX@PNIPAM-induced lesions to the tumor cells (Fig. 6e). Therefore, the antitumor effects of thermoresponsive drug delivery to mitochondria were consistently validated *in vitro* and *in vivo*.

4. Conclusion

We have developed a mitochondrial temperature-responsive drug delivery strategy for reversing DOX resistance in small-cell lung cancer. Compared with the nonthermoreponsive control, thermoresponsive nanocarriers could increase intracellular DOX levels, enhance the

mitochondrial targeting of DOX and facilitate tumor-specific accumulation of DOX. Consequently, thermoresponsive delivery of DOX to mitochondria reversed DOX resistance in the cellular and mouse model of DOX-resistant small-cell lung cancer. These results suggest that mitochondrial temperature-responsive nanocarrier is a promising tool for addressing drug resistance in cancer.

Declaration of competing interest

The authors declare no competing financial interest.

CRedit authorship contribution statement

Lifo Ruan: Methodology, Validation, Formal analysis, Investigation, Data curation, Writing – original draft, All the authors have analyzed the data and contributed to the figure preparation and manuscript revision. **Jun Chen:** Methodology, Investigation, Writing – review & editing, All the authors have analyzed the data and contributed to the figure preparation and manuscript revision. **Guangjun Nie:** Formal analysis, Supervision, Writing – review & editing, All the authors have analyzed the data and contributed to the figure preparation and manuscript revision. **Yi Hu:** Conceptualization, Methodology, Supervision, Funding acquisition, Writing – review & editing, All the authors have analyzed the data and contributed to the figure preparation and manuscript revision.

Acknowledgements

We are grateful to Beijing Natural Science Foundation (7212212), National Natural Science Foundation of China (11875269 and 21574136), and Hundred Talents Program of CAS for financial support.

Appendix A. Supplementary data

Supplementary data to this article can be found online at <https://doi.org/10.1016/j.bioactmat.2021.10.045>.

References

- N. Vasani, J. Baselga, D.M. Hyman, A view on drug resistance in cancer, *Nature* 575 (2019) 299–309.
- C.F. Higgins, Multiple molecular mechanisms for multidrug resistance transporters, *Nature* 446 (2007) 749–757.
- A.F. Gazdar, P.A. Bunn, J.D. Minna, Small-cell lung cancer: what we know, what we need to know and the path forward, *Nat. Rev. Cancer* 17 (2017) 725–737.
- R.W. Robey, K.M. Pluchino, M.D. Hall, A.T. Fojo, S.E. Bates, M.M. Gottesman, Revisiting the role of ABC transporters in multidrug-resistant cancer, *Nat. Rev. Cancer* 18 (2018) 452–464.
- Z.L. Johnson, J. Chen, Structural basis of substrate recognition by the multidrug resistance protein MRP1, *Cell* 168 (2017) 1075–1085.
- R.J. Youle, Mitochondria-striking a balance between host and endosymbiont, *Science* 365 (2019), eaaw9855.
- S. Vyas, E. Zaganjor, M.C. Haigis, Mitochondria and cancer, *Cell* 166 (2016) 555–566.
- T. Alexa-Stratulat, M. Pesic, A.C. Gasparovic, I.P. Trougakos, C. Riganti, What sustains the multidrug resistance phenotype beyond ABC efflux transporters? Looking beyond the tip of the iceberg, *Drug Resist. Updates* 46 (2019). UNSP 100643.
- Y.Y. Liu, J.W. Zhang, C.J. Zuo, Z. Zhang, D.L. Ni, C. Zhang, et al., Upconversion nano-photosensitizer targeting into mitochondria for cancer apoptosis induction and cyt c fluorescence monitoring, *Nano Res.* 9 (2016) 3257–3266.
- P. Hu, T. Wu, W.P. Fan, L. Chen, Y.Y. Liu, D.L. Ni, et al., Near infrared-assisted Fenton reaction for tumor-specific and mitochondrial DNA-targeted photochemotherapy, *Biomaterials* 141 (2017) 86–95.
- S. Louzoun-Zada, Q.Z. Jaber, M. Fridman, Guiding drugs to target-harboring organelles: stretching drug-delivery to a higher level of resolution, *Angew. Chem. Int. Ed.* 58 (2019) 15584–15594.
- D.B. Cheng, X.H. Zhang, Y.J. Gao, L. Ji, D.Y. Hou, Z.Q. Wang, et al., Endogenous reactive oxygen species-triggered morphology transformation for enhanced cooperative interaction with mitochondria, *J. Am. Chem. Soc.* 141 (2019) 7235–7239.
- T.J. Ji, D.S. Kohane, Nanoscale systems for local drug delivery, *Nano Today* 28 (2019) 100765.
- D.Q. Wang, H. Huang, M.X. Zhou, H.R. Lu, J. Chen, Y.T. Chang, et al., A thermoresponsive nanocarrier for mitochondria-targeted drug delivery, *Chem. Commun.* 55 (2019) 4051–4054.
- L.F. Ruan, M.X. Zhou, J. Chen, H. Huang, J.Y. Zhang, H.Y. Sun, et al., Thermoresponsive drug delivery to mitochondria in vivo, *Chem. Commun.* 55 (2019) 14645–14648.
- L.M. Yang, P. Gao, Y.L. Huang, X. Lu, Q. Chang, W. Pan, et al., Boosting the photodynamic therapy efficiency with a mitochondria-targeted nanophotosensitizer, *Chin. Chem. Lett.* 30 (2019) 1293–1296.
- X. Guo, X. Wei, Z. Chen, X. Zhang, G. Yang, S. Zhou, Multifunctional nanoplatforms for subcellular delivery of drugs in cancer therapy, *Prog. Mater. Sci.* 107 (2020) 100599.
- M. Wang, L. Ruan, T. Zheng, D. Wang, M. Zhou, H. Lu, et al., A surface convertible nanoplatform with enhanced mitochondrial targeting for tumor photothermal therapy, *Colloids Surf. B Biointerfaces* 189 (2020) 110854.
- Z. Lian, T.J. Ji, Functional peptide-based drug delivery systems, *J. Mater. Chem. B* 8 (2020) 6517–6529.
- Y.N. Li, T. Mei, S.P. Han, T. Han, Y.B. Sun, H. Zhang, et al., Cathepsin B-responsive nanodrug delivery systems for precise diagnosis and targeted therapy of malignant tumors, *Chin. Chem. Lett.* 31 (2020) 3027–3040.
- J. Zielonka, J. Joseph, A. Sikora, M. Hardy, O. Ouari, J. Vasquez-Vivar, et al., Mitochondria-targeted triphenylphosphonium-based compounds: syntheses, mechanisms of action, and therapeutic and diagnostic applications, *Chem. Rev.* 117 (2017) 10043–10120.
- V. Reshetnikov, S. Daum, C. Janko, W. Karawacka, R. Tietze, C. Alexiou, et al., ROS-responsive N-alkylaminofluorenes for cancer-cell-specific targeting of mitochondria, *Angew. Chem. Int. Ed.* 57 (2018) 11943–11946.
- M. Momcilovic, A. Jones, S.T. Bailey, C.M. Waldmann, R. Li, J.T. Lee, et al., In vivo imaging of mitochondrial membrane potential in non-small-cell lung cancer, *Nature* 575 (2019) 380–384.
- D. Chretien, P. Benit, H.H. Ha, S. Keipert, R. El-Khoury, Y.T. Chang, et al., Mitochondria are physiologically maintained at close to 50 °C, *PLoS Biol.* 16 (2018), e2003992.
- D. Wang, M. Zhou, H. Huang, L. Ruan, H. Lu, J. Zhang, et al., Gold nanoparticle-based probe for analyzing mitochondrial temperature in living cells, *ACS Appl. Bio Mater.* 2 (2019) 3178–3182.
- A. Sukhanova, S. Bozrova, P. Sokolov, M. Berestovoy, A. Karaulov, I. Nabiev, Dependence of nanoparticle toxicity on their physical and chemical properties, *Nanoscale Res. Lett.* 13 (2018) 44.
- H. Gao, Y. Bi, X. Wang, M. Wang, M.X. Zhou, H.R. Lu, et al., Near-infrared guided thermal-responsive nanomedicine against orthotopic superficial bladder cancer, *ACS Biomater. Sci. Eng.* 3 (2017) 3628–3634.
- M.X. Zhou, X.C. Zhang, J. Xie, R.X. Qi, H.R. Lu, S. Loporatti, et al., pH-sensitive poly(beta-amino ester)s nanocarriers facilitate the inhibition of drug resistance in breast cancer cells, *Nanomaterials* 8 (2018) 952.
- M.X. Zhou, H. Huang, D.Q. Wang, H.R. Lu, J. Chen, Z.F. Chai, et al., Light-triggered PEGylation/dePEGylation of the nanocarriers for enhanced tumor penetration, *Nano Lett.* 19 (2019) 3671–3675.
- Z.J. Wang, X. Kuang, J. Shi, W.L. Guo, H.Z. Liu, Targeted delivery of geranylgeranylacetone to mitochondria by triphenylphosphonium modified nanoparticles: a promising strategy to prevent aminoglycoside-induced hearing loss, *Biomater. Sci.* 5 (2017) 1800–1809.
- S. Arai, M. Suzuki, S.J. Park, J.S. Yoo, L. Wang, N.Y. Kang, et al., Mitochondria-targeted fluorescent thermometer monitors intracellular temperature gradient, *Chem. Commun.* 51 (2015) 8044–8047.
- S.E. Mirski, J.H. Gerlach, S.P. Cole, Multidrug resistance in a human small cell lung cancer cell line selected in adriamycin, *Cancer Res.* 47 (1987) 2594–2598.
- G. Kibria, H. Hatakeyama, K. Akiyama, K. Hida, H. Harashima, Comparative study of the sensitivities of cancer cells to doxorubicin, and relationships between the effect of the drug-efflux pump P-gp, *Biol. Pharm. Bull.* 37 (2014) 1926–1935.
- S.P.C. Cole, G. Bhardwaj, J.H. Gerlach, J.E. Mackie, C.E. Grant, K.C. Almquist, et al., Overexpression of a transporter gene in a multidrug-resistant human lung-cancer cell-line, *Science* 258 (1992) 1650–1654.
- B.G. Peterson, K.W. Tan, B. Osa-Andrews, S.H. Iram, High-content screening of clinically tested anticancer drugs identifies novel inhibitors of human MRP1 (ABCC1), *Pharmacol. Res.* 119 (2017) 313–326.
- G. Minotti, P. Menna, E. Salvatorelli, G. Cairo, L. Gianni, Anthracyclines: molecular advances and pharmacologic developments in antitumor activity and cardiotoxicity, *Pharmacol. Rev.* 56 (2004) 185–229.
- Y. Pommier, Y.L. Sung, S.Y.N. Huang, J.L. Nitiss, Roles of eukaryotic topoisomerases in transcription, replication and genomic stability, *Nat. Rev. Mol. Cell Biol.* 17 (2016) 703–721.
- F.S. Carvalho, A. Burgeiro, R. Garcia, A.J. Moreno, R.A. Carvalho, P.J. Oliveira, Doxorubicin-induced cardiotoxicity: from bioenergetic failure and cell death to cardiomyopathy, *Med. Res. Rev.* 34 (2014) 106–135.